The Crystal Structure of N^{10}-Formyltetrahydrofolate Synthetase from *Moorella thermoacetica*[†,‡]

Ramin Radfar,[§] Ronald Shin,[§] George M. Sheldrick,[||] Wladek Minor,[⊥] Charles R. Lovell,[#] Jerome D. Odom,[§] R. Bruce Dunlap,[§] and Lukasz Lebioda*[,§]

Departments of Chemistry and Biochemistry and of Biological Sciences, University of South Carolina, Columbia, South Carolina 29208, Department of Molecular Physiology and Biological Physics, University of Virginia, Charlottesville, Virginia 22901, and Institut für Anorganiche Chemie, University of Göttingen, D-37077, Göttingen, Germany

Received December 6, 1999; Revised Manuscript Received January 31, 2000

ABSTRACT: The structure was solved at 2.5 Å resolution using multiwavelength anomalous dispersion (MAD) scattering by Se-Met residues. The subunit of N^{10}-formyltetrahydrofolate synthetase is composed of three domains organized around three mixed β-sheets. There are two cavities between adjacent domains. One of them was identified as the nucleotide binding site by homology modeling. The large domain contains a seven-stranded β-sheet surrounded by helices on both sides. The second domain contains a five-stranded β-sheet with two α-helices packed on one side while the other two are a wall of the active site cavity. The third domain contains a four-stranded β-sheet forming a half-barrel. The concave side is covered by two helices while the convex side is another wall of the large cavity. Arg 97 is likely involved in formyl phosphate binding. The tetrameric molecule is relatively flat with the shape of the letter X, and the active sites are located at the end of the subunits far from the subunit interface.

Tetrahydrofolate (THF)[1] and its derivatives are the biologically active forms of folic acid, a four-electron oxidized form of THF. They are specialized cosubstrates for a variety of enzymes involved in one-carbon metabolism. THF reacts in an ATP-dependent manner with formate in the following reaction catalyzed by formyltetrahydrofolate synthetase (FTHFS) (EC 6.3.4.3).

$$\mathrm{HCOOH + Mg{\cdot}ATP + THF \rightleftarrows 10\text{-formyl-THF} + Mg{\cdot}ADP + P_i}$$

The catalyzed reaction proceeds via the formation of a tightly bound formyl phosphate intermediate produced by nucleophilic attack of formate on the γ-phosphate of Mg·ATP (*1*). Subsequently, the N^{10} of THF affords nucleophilic attack on the formyl group of formyl phosphate, resulting in the formation of the final product, 10-formyl-THF, and the release of products.

The enzyme, present at high levels in the acetogenic and purinolytic bacteria, is involved in a C_1 carbon fixation process for cellular biosynthesis. It has been purified to homogeneity from *Moorella thermoacetica* (*2*) (previously referred to as *Clostridium thermoaceticum*), *Clostridium acidiurici* (*3*), and *Clostridium cylindrosporum* (*3*). These FTHFSs have been extensively studied and found to be remarkably similar in chemical, physical, and enzymatic properties (*4*) as can be expected from the highly conserved sequence (Figure 1). All known clostridial FTHFSs are homotetramers of molecular mass 240 kDa (*5*). *C. acidurici* and *C. cylindrosporum* possess the ability to ferment purines, which are utilized as a source of carbon and nitrogen. *M. thermoacetica* can produce acetate from hydrogen and carbon dioxide (*6*).

In contrast, the enzyme from eukaryotes, referred to as C-1 H_4folate synthase, has a more complex structure. In addition to the N^{10}-formylH_4folate synthetase activity contained in the C-terminal 70 kDa domain, these proteins contain $N^{5,10}$-methenylH_4folate cyclohydrolase (EC 3.5.4.9) and $N^{5,10}$-methyleneH_4folate dehydrogenase (EC 1.5.1.5) activities (*7*). One of the biochemical roles of this system is to maintain formaldehyde and formate in chemically poised states, not so reactive as to poise a toxic threat to the cell but available for some biochemical processes. The structure of the N-terminal domain of C-1 H_4folate synthase has been previously reported by Cygler and his collaborators (*8*). Here we report the first determination of the 3D structure of FTHFS.

[†] This work was supported by NSF Grant MCB-9873606. Some instrumentation used in this research was purchased with NSF Grant BIR 9419866 and DOE Grant DE-FG-95TE00058. Use of the Argonne National Laboratory Structural Biology Center beamlines, at the Advanced Photon Source, was supported by the U. S. Department of Energy, Office of Science, under Contract W-31-109-ENG-38.

[‡] The PDB file of the crystal structure of N^{10}-formyltetrahydrofolate synthetase is deposited in the Protein Data Bank under accession code 1EG7.

* To whom correspondence should be addressed at the Department of Chemistry and Biochemistry, University of South Carolina, 730 S. Main St., Columbia, SC 29208. E-mail: lebioda@psc.sc.edu.

[§] Department of Chemistry and Biochemistry, University of South Carolina.

[||] Institut für Anorganiche Chemie, University of Göttingen.

[⊥] Department of Molecular Physiology and Biological Physics, University of Virginia.

[#] Department of Biological Sciences, University of South Carolina.

[1] Abbreviations: Se-Met, selenomethionine; MAD, multiwavelength anomalous dispersion; FTHFS, formyltetrahydrofolate synthetase; THF, tetrahydrofolate; KMB, potassium maleate buffer; EDTA, ethylenediaminetetraacetic acid; F_o, observed structure factor; F_c, calculated structure factor; f'', imaginary component of the anomalous scattering factor; V_m, ratio of unit cell volume and the molecular weight.

10.1021/bi992790z CCC: $19.00
Published on Web 03/15/2000

FIGURE 1: Amino acid sequence alignment of FTHFS from *M. thermoacetica* (M.TH), *C. acidiurici* (C.AC), *C. cylindrosporum* (C.CY), *Escherichia coli* ATPase (ATPase_E.C), and *Azotobacter vinelandii* nitrogenase Fe protein (Ntrgen_A.V). Conserved residues among FTHFS sequences are shown in blue and those identical in ATP binding proteins in red. The conserved segment between FTHFS and methylene-H_4 reductase is shown in green. α-Helices and *β*-strands are indicated by solid lines and arrows, respectively.

MATERIALS AND METHODS

Selenomethionine FTHFS. The plasmid from the *Escherichia coli* strain Y1, which expresses the protein, contains a 4.3 kb insert derived from PCRL47 (*9*) and was isolated using an alkaline lysis procedure (*10, 11*). The lysate was centrifuged at 13000*g* for 10 min, followed by the removal of impurities using 1:1 phenol−chloroform. The plasmid DNA was then precipitated with ice-cold 95% ethanol and centrifuged at 13000*g* for 10 min. The supernatant was discarded, and the pellets were rinsed again with ice-cold 95% ethanol. Each of the pellets was then suspended in 50 μL of 10 mM TRIS (pH 8.0) and 1 mM EDTA.

Following isolation, 5 ng of the DNA was added to 100 μL of competent methionine auxotroph *E. coli* strain DL41 in a sterile culture tube. After incubation on ice for 1 h, 1 mL of LB broth was added, along with 100 μL of 2 M glucose and 15 μg of tetracycline. The culture tube was incubated at 37 °C for 3 h. Then 100 μL aliquots of the bacterial suspension were spread plated on LB-Agar plates containing 15 μg mL^{-1} tetracycline, and incubated at 37 °C for 24 h. The colonies found on the plates contained the FTHFS-producing plasmid. Ten milliliters of defined medium containing 15 μg mL^{-1} tetracycline and 50 μg L^{-1} D,L-selenomethionine was inoculated with individual colonies of the recombinant bacteria. After 12 h, the tubes containing the bacterial suspension were added to individual Erlenmeyer flasks containing 1 L each of the sterile medium. After the Abs_{600} reached 2.5, the culture was harvested by centrifugation at 6000*g* for 10 min, and the cells were lysed using sonication in an ice/95% ethanol bath for 10 min. Following

sonication, the lysate was centrifuged at 10000*g* for 30 min, and the pellet was discarded. Specific activity assays showed a level of activity that was within 5% of that of the wild-type enzyme. Graphite-furnace atomic absorption spectroscopy showed the complete replacement of Met by Se-Met.

Purification and Crystallization. Our FTHFS purification procedure takes advantage of the fortuitous binding of heparin by this enzyme (*12*). After cultivation in LB broth containing tetracycline, the culture was harvested and the cell pellet suspended in 50 mM potassium maleate buffer, pH 7.0 (KMB). Cell lysis was achieved by sonication and the cellular debris pelleted by centrifugation. The cleared extract was adjusted to 0.4 mg mL^{-1} streptomycin sulfate and stirred gently at 4 °C for 30 min. Nucleic acids and some contaminating proteins were removed by centrifugation, and the supernatant was loaded onto a heparin−agarose column equilibrated with KMB. After the column was washed with KMB, the proteins were eluted with a linear gradient from 0 to 0.4 M KCl in KMB. Peak FTHFS fractions were pooled and loaded onto a phenyl Sepharose column previously equilibrated with 0.7 M ammonium sulfate in KMB. The proteins were eluted using a linear gradient from 0.7 to 0 M ammonium sulfate in KMB. FTHFS in the peak fractions after this purification step was typically greater than 95% pure.

Se-Met FTHFS was crystallized by the hanging-drop vapor-diffusion method using previously described conditions (*13*). After 2 weeks, crystals as large as 0.6 mm × 0.5 mm × 0.2 mm were found. The crystals belong to space group *R32* with unit cell dimensions of $a = 160.88$ Å and $c = 256.12$ Å with 2 subunits per asymmetric part of the unit cell ($V_m = 2.3$ Å^3 Da^{-1}; 46.5% solvent content).

X-ray Data Collection and Processing. Multiwavelength diffraction data for MAD phasing of the Se-Met FTHFS were collected at the Structural Biology Center (SBC) beamline at the Advanced Photon Source (APS), Argonne National Laboratory (ANL). Data sets were collected at four different wavelengths: the low- and high-energy remote (λ_1 and λ_4), the inflection point (λ_2), and the peak of f'' (λ_3). The data were collected as 1° oscillation frames from a single crystal frozen at 100 K. Cryogenic conditioning of the Se-Met FTHFS crystals was achieved by soaking the crystals in 22% glycerol-enriched mother liquor. All data were processed with the HKL 2000 system (*14*) (Table 1). There are 14 (seleno)-methionines, containing anomalous scatterers, per subunit of *M. thermoacetica* FTHFS; 2 subunits per asymmetric part of the unit cell make it a 28-atom problem. To obtain the positions of Se atoms, the four-wavelength data were combined together using the local scaling option of the SOLVE package (*15*). The estimates of structure factors of the anomalous scatterers (F_a's) were used as the input to the SHELXD (*16*) program and yielded the positions of all 28 Se atoms. The average deviations of the original positions of the Se atoms from those from the final model were 0.25 Å for subunit A and 0.46 Å for subunit B. The preliminary MAD phases were calculated by the maximum-likelihood algorithm implemented in MLPHARE (*17*) using the Se sites. Solvent flattening and histogram matching were applied to improve the initial phases using the DM program (*18*) from the CCP4 package (*17*). The structure refinement was carried out against the data set collected at $\lambda = 1.04189$ Å, which had the best statistics.

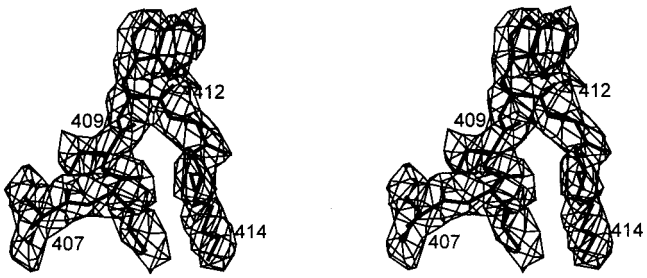

FIGURE 2: Stereoview of a representative portion of the MAD-phased map. Based on the sequence, serine 409 should be followed by glutamate, valine, and then tryptophan 412, but electron density after serine 409 shows a clear side chain density for tryptophan 412. Omit maps in this region are very similar.

RESULTS AND DISCUSSION

MAD Phasing, Model Building, and Refinement. Data were collected at four wavelengths, and the MAD data sets were

Table 1: Data Collection and Refinement Statistics of Se-Met FTHFS

Data Collection				
wavelength (Å)	λ_1 (1.04189)	λ_2 (0.97938)	λ_3 (0.97922)	λ_4 (0.93928)
resolution range (Å)	10.0−2.49	10.0−2.76	10.0−2.45	10.0−2.22
all reflections	194269	179626	176111	193747
unique reflections	43717	41602	41052	48310
completeness (%)	97.2	90.9	89.5	78.1
R_{sym}	0.046	0.069	0.085	0.065
mosaicity	0.748	0.715	0.712	0.689
mean figure of merit after MLPHARE (10.0−3.00 Å)			0.68	

Refinement Statistics	
resolution range	20.0−2.5 Å
reflections ($\|F\| > 3\sigma$)	40064 (90.7%)
non-hydrogen protein atoms	8264 (1097 residues)
water molecules	269
R-factor (%)	24.5
R_{free} (%)	29.7
Ramachandran analysis	939 non-Gly and non-Pro residues
most favored	81.3% (763 residues)
additional allowed	17.1% (161 residues)
generously allowed	1.1% (10 residues)
nonallowed	0.5% (5 residues)

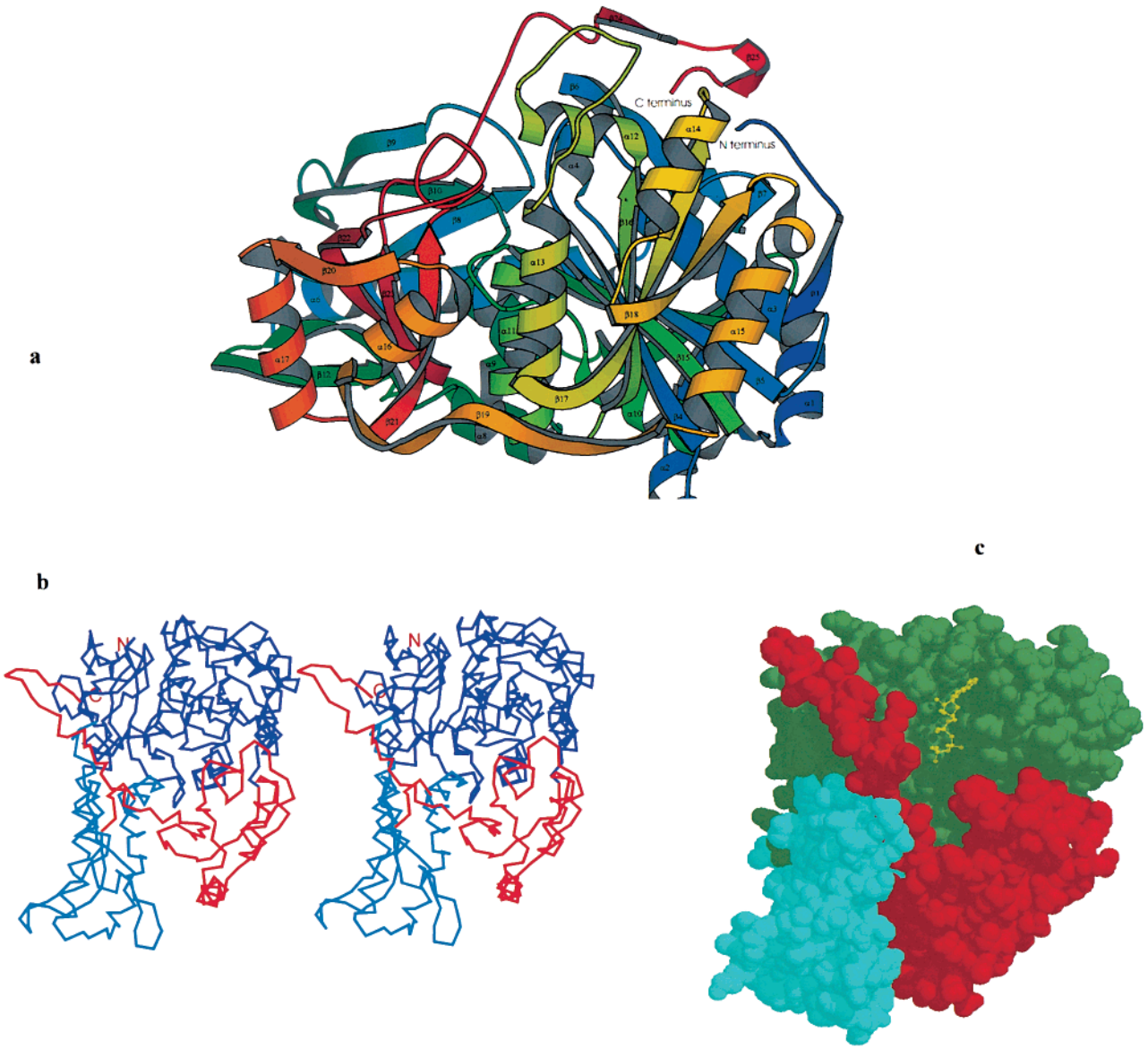

FIGURE 3: (a) Ribbon diagram of the FTHFS protomer from *Moorella thermoacetica* with rainbow coloring following residue numbers. The N- and C-termini are labeled and secondary structure elements numbered. (b) Stereo diagram of C_α trace of the FTHFS. Domains 1, 2, and 3 are shown in blue, cyan, and red, respectively. The position of a hexapeptide conserved between FTHFS and methylene-THF reductase is shown in orange. (c) The surface of the protomer with the modeled position of ATP marking the putative active site. The view is approximately at the same angle as in (b).

treated as conventional heavy atom derivatives to exploit the dispersive differences caused by different wavelengths as a source of phase information (*19*). The resulting electron density was readily interpretable with well-defined secondary structure and visible side chains. Figure 2 shows a representative portion of the MAD map. For most of the molecule, the electron density was excellent, and the model of two subunits present per asymmetric part of the unit cell, referred to below as A and B, was built using the CHAIN (*20*) software. The model includes residues 7−409, and 412−557, covering 98.2% of the sequence. There was no density for residues 410 and 411. Electron density maps in this region are continuous, and at 1σ contouring level, a clear side chain density can be seen for Trp 412 after Ser 409 (Figure 2). It is thus possible that the clone used had these residues deleted. If so, this deletion does not affect catalytic properties of the enzyme (vide infra). The quality of electron density for a large portion of subunit B is clearly lower than that for the corresponding part of subunit A, and the refined temperature factors are higher. A comparison of subunit B with A showed that the majority of residues with high temperature factors are located in domain 1 (80%) and the rest in an adjacent loop of domain 3. Domain 1 is the possible binding site for nucleotide triphosphate, and its flexibility may play a role in folate binding.

The initial model was improved by the simulated annealing method implemented in X-PLOR (*21*) using a total of 40 064 reflections. The free *R*-factors were used to justify each refinement step with 5% of the reflections set aside for R_{free} calculations. After several cycles of coordinate adjustments using the programs CHAIN and X-PLOR, the resulting *R*-factor dropped from 43% to 28.5%. In further refinement cycles, carried out with CNS *(22)*, the 2-fold noncrystallography symmetry restraints were removed and water molecules added. The incorporation of water molecules reduced the *R*-factor to 24.5% and the free *R*-factor from 32.3% to

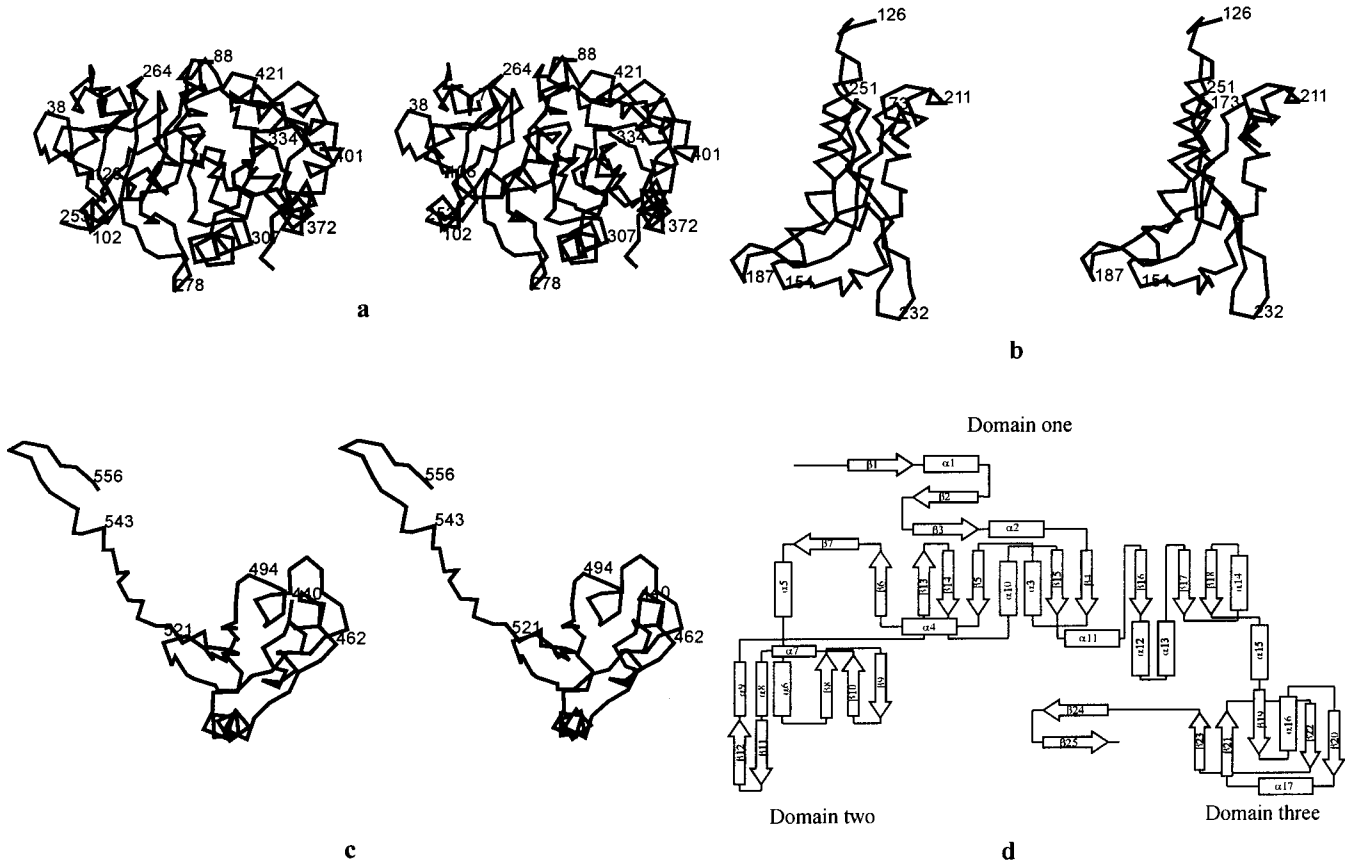

FIGURE 4: Stereoview of domains 1, 2, and 3 as (a), (b), and (c), respectively. Topology diagram of the entire subunit in (d).

29.7%. We believe that this relatively high *R*-factor is a result of partial disorder of subunit B, vide infra.

The reported FTHFS model for 2 subunits contains 8264 atoms, 11 sulfates, 2 *cis*-prolines (residue 121), and 269 water molecules. Program PROCHECK (*23*) was used to determine the number of residues in different regions of a Ramachandran plot for dimer, and more than 81% of the residues were found to have conformation in the "most favored" regions (Table 1).

Overall Structure of FTHFS. The ribbon diagram of the FTHFS polypeptide chain and the stereo diagram of the C_α trace are shown in Figure 3a and 3b, respectively. The FTHFS protomer containing 559 residues consists of one large and two smaller domains. Domain 1 includes residues 7−120 and 254−431. The core of this domain is formed from a central sheet with seven parallel strands (β4, β5, β14−17). Strand β13 is almost perpendicular to the plane of the core sheet and links domains 2 to 1. The core sheet is surrounded by eight α-helices (α1, α3, α10−15), three β-strands (β1−3), and the α/β motif (α4−5, β6−7) that connects domains 1 to 2. Domain 2 includes residues 131−250 and is composed of five β-strands (β8−12) and four α-helices (α6−9). Domain 3 with 124 residues (433−557) contains six β-strands (β19−24) and two α-helices (α16−17). The deep cleft between the domains is likely the active site pocket and the binding site for ATP, formate, and THF (Figure 3c). The N- (residue 7) and C-termini (residue 557) are just 16 Å apart; the subunit possesses approximate dimensions of 70 Å × 50 Å × 40 Å. A stereo diagram of a C_α trace for each domain and the overall topology diagram are shown in Figure 4a and 4b. A search for proteins with similar fold was carried out using a DALI (*24*) server. The highest match found was for two ATP binding proteins, dethiobiotin synthetase (*25*) and nitrogenase iron protein (*26*). However, the topologies of these proteins are different, and there is no indication of common ancestry.

Quaternary Structure of FTHFS. The tetrameric molecule (Figure 5) shows an unusual quaternary structure with four subunits arranged approximately in the same plane with the shape of letter "X". The interface between two subunits forming the tightly bound dimer and related by crystallographic 2-fold symmetry is clearly different from that connecting dimers related by noncrystallographic 2-fold symmetry. The tight dimer is formed by hydrophobic interaction between the side chains of β-strand 9, α-helix 9, and β-strand 24. The amino acid sequence at the interface region is highly conserved between bacterial FTHFS, but for the mammalian enzyme, only 35% of residues were conserved. This suggests that C-1 H_4folate synthase dimerizes in a different fashion than FTHFS. Dimer and tetramer formation decreases the accessible surface by 2890 and 3456 Å^2 per subunit, which is 12.7% and 15.1% of the total surface of the subunit, respectively. FTHFSs from clostridial sources bind THF only in the tetrameric state (*27*); thus, the appropriate active site conformation is induced upon the association of monomers.

Active Site. FTHFS amino acid sequence comparison (*9*) with some known ATP binding proteins suggests that the ATP binding site involves residues 58−85 (Figure 1). To determine the nucleotide binding site in the structure, the ATP binding domains of *Escherichia coli* ATPase (*28*) (residues 163−185) and *Azotobacter vinelandii* nitrogenase Fe protein (*26*) (residues 3−26) were superimposed onto FTHFS (residues 58−85). Figure 6a shows the superimposi-

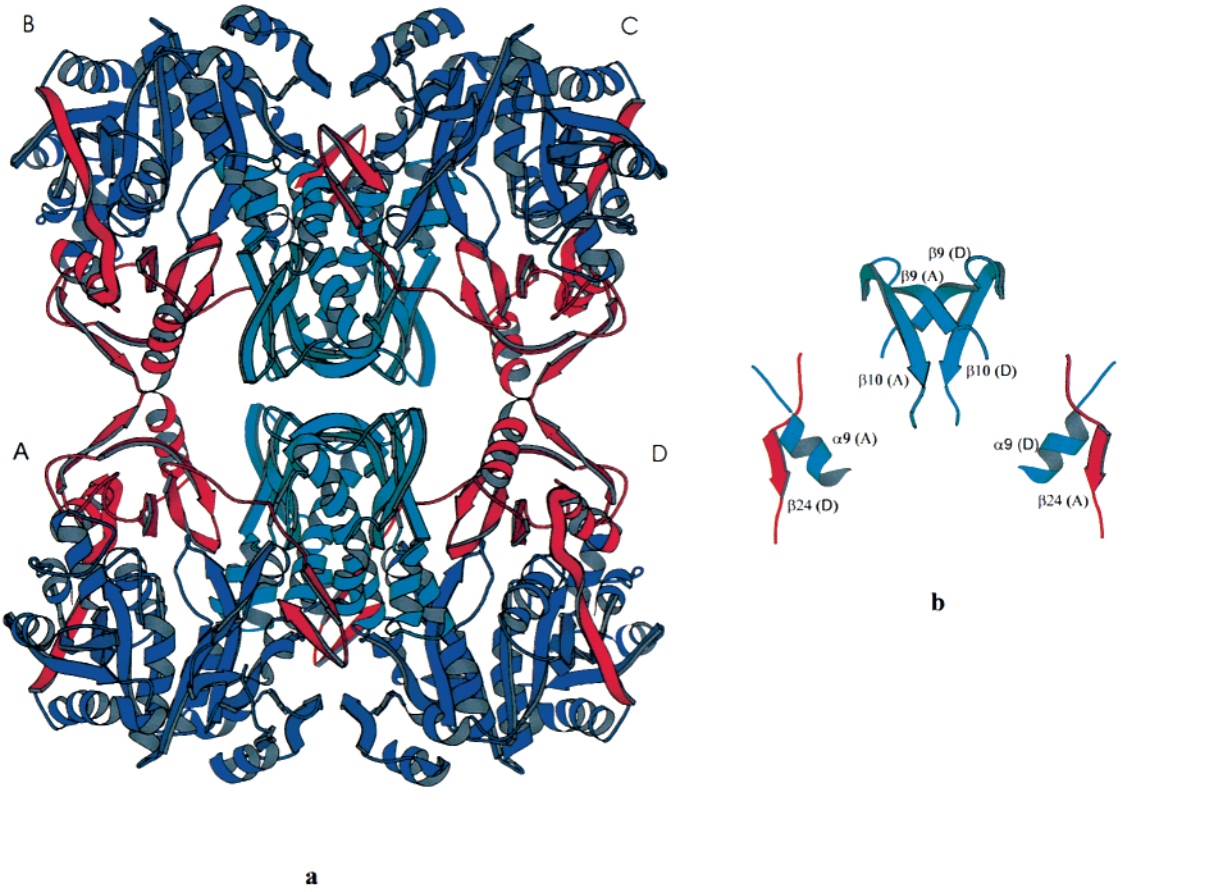

FIGURE 5: (a) Arrangement of subunits in the quaternary structure of FTHFS. Subunits A/B (and C/D) are related by 2-fold noncrystallographic symmetry (along the horizontal axis in the plane of the picture) and A/D (and B/C) by a crystallographic 2-fold symmetry approximately along the vertical axis. The tetramer has approximate dimensions of 109 Å × 97 Å × 45 Å. Domains 1, 2, and 3 are shown in purple, blue, and red, respectively. 80% of the residues with high temperature factors are located in domain 1. (b) β-Strands 9, 10, and 24 and α-helix 9 from the subunit A/D interface.

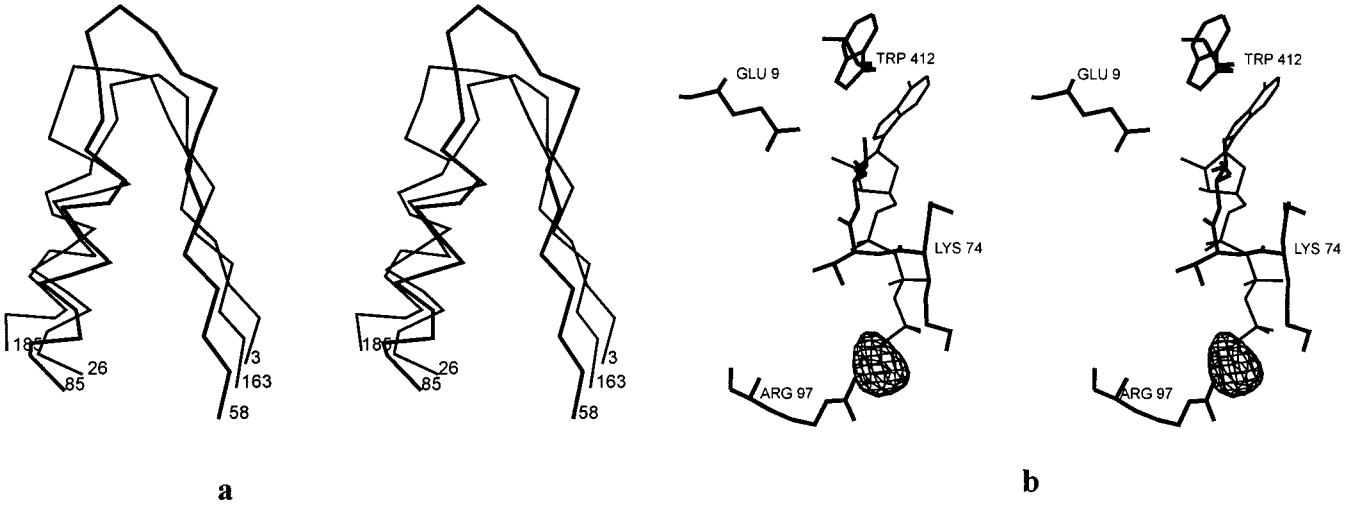

FIGURE 6: (a) Superposition of C_α atoms of FTHFS (58−85), *Azotobacter vinelandii* nitrogenase Fe protein (3−26), and *Escherichia coli* ATPase (163−185). FTHFS is drawn in boldface. (b) Stereo diagram of the nucleotide binding site modeled based on comparison with ATP binding proteins. Calculated $|F_o| - |F_c|$ map contoured at 3σ shows a strong peak which most likely represents a sulfate ion density and is likely the binding site for the formyl phosphate catalytic intermediate.

tion of these segments. Calculated rms deviations of C_α positions for residues 73−81 of FTHFS are 0.50 and 0.35 Å for nitrogenase and ATPase, respectively. These sites suggest the location of the putative active site and are located at each corner of the tetramer so the FTHFS molecule may bind four nucleotide triphosphates. An examination of the ATP environment (Figure 6b) suggests that Trp 412 stabilizes the adenosine ring with a stacking interaction, the Glu 9 side chain interacts with a hydroxyl group of the ribose ring, the Thr 76 hydrogen bonds with the adenosine ring, and Thr 75 and Lys 74 bind the triphosphate moiety. The present structure has a two-residue deletion just prior to Trp 412. These two residues are present in all the other sequences in the NCBI database. A deletion of these residues may have

an effect on positioning of Trp 412. However, since this deletion does not affect the catalytic function, the role of Trp 412 may not be that important. For the enzyme to carry out the phosphorylation of formate, the binding site of formate should be close to the triphosphate moiety. Examination of the $|F_o| - |F_c|$ map at 3.0 σ contouring level showed a strong peak most likely corresponding to a bound sulfate ion, approximately 2.6 Å apart from the Arg 97 side chain and partially overlapping with the modeled position of the triphosphate moiety (Figure 6b). It is likely that this sulfate position corresponds to the formyl phosphate binding site.

Amino acid sequence analysis showed that the only folate binding enzyme with a sequence related to the FTHFS is methylene-THF reductase (*9*). In that study, residues 145−150 of methylene-THF reductase were found to be exactly the same as residues 197−202 of FTHFS from different sources and almost the same as those in C-1 FTHFS. Methylene-THF reductase and FTHFS have completely different folds as the former has the 8-fold $\beta\alpha$-barrel fold (TIM-barrel) with the conserved segment located in one of the central β-strands. Nevertheless, this segment in FTHFS is located in the active site (Figure 3b), and its conservation apparently results from convergent evolution. The FTHFS subunit has two large cavities located very close to one another. The one next to the C- and N-termini contains the modeled nucleotide and formate binding site. The conserved segment is located between these two cavities with the hexapeptide sandwiched between α-helix 6, β-strand 8, and the long C-terminal coil connecting β-sheets 23 and 24.

Kinetics. Previous kinetic studies have shown that the active form of the nucleotide is a Mg^{2+}−nucleotide complex (*29*). As part of our studies of the catalytic mechanism of this enzyme, V_{max} and K_m values were measured for both Se-Met and wild-type FTHFS. At different THF, ATP, Mg^{2+}, and formate concentrations, the Se-Met FTHFS exhibited similar behavior to the wild type. Se-Met FTHFS did differ from the wild-type enzyme in that the protein retains 100% of its activity when equimolar amounts of Ca^{2+} were substituted for Mg^{2+}, as opposed to 70% for the wild type. These studies also showed that if indeed the Se-Met FTHFS had residues 410−411 deleted, the deletion did not affect its catalytic performance.

ACKNOWLEDGMENT

We acknowledge Adam Leaphart and Dr. Yung Pin Chen for assistance with FTHFS purification.

REFERENCES

1. Mejillano, M. R., Jahansouz, H., Matsunaga, T. O., Kenyon, G. L., and Himes, R. H. (1989) *Biochemistry 28*, 5136−5145.
2. Ljungdahl, L. G., Brewer, J. M., Neece, S. H., and Fairwell (1970) *J. Biol. Chem. 245*, 4791−4797.
3. Rabinowitz, J. C., and Picer, W. E., Jr. (1962) *J. Biol. Chem. 237*, 2898−2902.
4. Lovell, C. R., Przybyla, A., and Ljungdahl, L. G. (1988) *Arch. Microbiol. 149*, 280−285.
5. MacKenzie, R. E., and Rabinowitz, J. C. (1971) *J. Biol. Chem. 246*, 3731−3736.
6. Wood, H. G., and Ljungdahl, L. G. (1991) in *Variations in Autotrophic Life*, *Autotrophic character of the acetogenic bacteria* (Shively, J. M., and Barton, L. L., Eds.) pp 201−250, Academic Press, New York.
7. Kounga, K., Song, S., Haslam, G. C., and Himes, R. H. (1996) *Biochim. Biophys. Acta 1296*, 112−120.
8. Allaire, M., Li, Y., MacKenzie, R. E., and Cygler, M. (1998) *Structure 6*, 173−182.
9. Lovell, C. R., Przybyla, A., and Ljungdahl, L. G. (1990) *Biochemistry 29*, 5687−5694.
10. Birnboim, H. C., and Doly, J. (1979) *Nucleic Acids Res. 7*, 1513.
11. Ish-Horowicz, D., and Burke, J. F. (1981) *Nucleic Acids Res. 9*, 2989.
12. Staben, C., Whitehead, T. R., and Rabinowitz, J. C. (1987) *Anal. Biochem. 162*, 257−264.
13. Lewinski, K., Hui, Y., Jakob, C. G., Lovell, C. R., and Lebioda, L. (1993) *J. Mol. Biol. 229*, 1153−1156.
14. Otwinowski, Z., and Minor, W. (1997) *Methods Enzymol. 276*, 307−326.
15. Terwilliger, T. C., and Berendzen, J. (1999) *Acta Crystallogr. D55*, 849−861.
16. Sheldrick, G. M. (1998) SHELX: applications to macromolecules. in *Direct Methods for Solving Macromolecular Structures* (Fortier, S., Ed.) pp 401−411 Kluwer Academic Publishers, Dordrecht, Holland.
17. Collaborative computational project, Number 4 (1994) *Acta Crystallogr. D50*, 760−763.
18. Cowtan, K. D. (1994) *Jt. CCP4 ESF-EACBM Newslett. Protein Crystallogr. 31*, 34−38.
19. Terwilliger, T. C. (1994) *Acta Crystallogr. D50*, 17−23.
20. Sack, J. S., and Quiocho, F. A. (1997) *Methods Enzymol. 277*, 158−173.
21. Brunger, A. T., Krukowski, A., and Erickson, J. (1989) *Acta Crystallogr. A45*, 50−61.
22. Brunger, A. T., Adams, P. D., Clore, G. M., Delano, W. L., Gros, P., Grosse-Kunstleve, R. W., Jiang, J. S., Kuszewski, J., Nilges, M., Pannu, N. S., Read, R. J., Rice, L. M., Simonson, T., and Warren, G. L. (1998) *Acta Crystallogr. D54*, 905−921.
23. Laskowski, R. A., MacArthur, M. W., Moss, D. S., and Thornton, J. M. (1993) *J. Appl. Crystallogr. 26*, 283−291.
24. Holm, L., and Sander, C. (1998) *Nucleic Acids Res. 26*, 316−319.
25. Sandalova, T., Schneider, G., Kack, H., and Lindqvist, Y. (1999) *Acta Crystallogr. D55*, 610−624.
26. Schlessman, J. L., Woo, D., Joshua-Tor, L., Howard, J. B., and Rees, D. C. (1998) *J. Mol. Biol. 280*, 669−685.
27. Mayer, F., Elliott, J. I., Sherod, D., and Ljungdahl, L. G. (1982) *Eur. J. Biochem. 124*, 397−404.
28. Gay, N. J., and Walker, J. E. (1981) *Nucleic Acids Res. 9*, 2187−2194.
29. Song, S., Velde, D. V., Gunn, C. W., and Himes, R. H. (1994) *Biochemistry 33*, 693−698.

BI992790Z